DOI:10.25092/baunfbed. 996414 *J. BAUN Inst. Sci. Technol., 24(2), 497-514, (2022)*

Static analysis of cantilever beam with geometrical discontinuity by Carrera Unified Formulation

Esra Eylem KARATAŞ[1*]

[1]*Gaziantep Üniversitesi, Mühendislik Fakültesi, İnşaat Mühendisliği Bölümü, Gaziantep, Türkiye*

Geliş Tarihi (Received Date): 16.09.2021
Kabul Tarihi (Accepted Date): 01.03.2022

Abstract

This paper presents a numerical solution for static analysis of a rectangular cantilever beam with different sizes of a hole on its cross-section subjected to vertical concentrated load. Carrera Unified Formulation (CUF) is used by employing both N-OrderTaylor type expansion (TE) and Lagrange type expansion (LE). The influence of both these different refined beam models and the different sizes of hole on the evaluation of the stress components on the cross-section along the thickness is examined. First, with the convergence study, a comparison is performed with the results obtained from the exact solution. Then, a rectangular cantilever beam with compact cross-section subjected to vertical concentrated load is considered. Finally, the presence of a hole with different radius sizes on its cross-section subjected to the same loading is discussed.

Keywords: *Refined beam models, unified formulation, CUF, finite element method, hole.*

Geometrik süreksizliğe sahip konsol kirişin Carrera birleşik formülasyonu ile statik analizi

Öz

Bu çalışma, dikey tekil yük etkisinde ve kesitinde boyutları farklı olacak şekilde bir delik içeren dikdörtgen kesitli konsol bir kirişin statik analizi için sayısal bir çözüm sunmaktadır. N. mertebeden Taylor açılımı (TE) ve Lagrange açılımı (LE) uygulanarak Carrera Birleşik Formulasyonu (CUF) kullanılmıştır. Hem her iki geliştirilmiş kiriş teorisinin hem de farklı boyutlardaki deliğin, kesit üzerinde kalınlık boyunca gerilme

[*]Esra Eylem KARATAŞ, ekaratas@gantep.edu.tr , https://orcid.org/0000- 0003-1396-2463.

bileşenleri üzerine etkisi incelenmiştir. İlk olarak, bir yakınsama ve kesin çözümden elde edilen sonuçlar ile bir karşılaştırma çalışması yapılmıştır. Daha sonra, tekil yük etkisinde ve kesitinde delik içermeyen dikdörtgen kesitli konsol kiriş ele alınmıştır. Son olarak da, aynı yük etkisi altında kesitte farklı yarıçaplara sahip delik olması durumu ele alınmıştır.

Anahtar kelimeler: *Geliştirilmiş kiriş modelleri, birleşik formulasyon, CUF, sonlu eleman metodu, delik.*

1. Introduction

Beam structures are extensively used in many engineering applications, such as blades and aircraft wings in aerospace engineering, and in arches, columns and truss members in civil engineering. For this reason, a large number of beam theories have been developed. The most well-known classical 1D models made of isotropic materials are the Euler–Bernoulli and Timoshenko theories. Euler–Bernoulli theory does not account for transverse shear deformations. However, it yields reasonably good results for slender beams. The Timoshenko beam theory provides uniform shear distribution along the cross section of the beam. However, the shear predicted by this theory should be corrected by using a shear correction factor. There are many methods to compute the shear correction factor in the literature [1-9]. The common feature of the Euler–Bernoulli and Timoshenko theories is that neither can consider non-classical effects such as in-plane deformations, warping, torsion-bending coupling, and localized boundary conditions either geometrical or mechanical [10]. Such effects often result from the fact that the material is anisotropic, and that the cross-section of the structural element is thin-walled and has a small slenderness ratio.

Refined and advanced beam theories are necessary in order to overcome the drawbacks of classical beam theories. These beam theories take into account different approaches including the introduction of shear correction factors, the use of cross-sectional warping and distortion, variational asymptotic solution (VABS), generalised beam theory (GBT) and higher-order beam models. In the literature, publications that consider these approaches include: [11-21].

The present work proposes a systemic manner of formulating axiomatically refined beam models. Via concise notation for the kinematic field, the governing differential equations and the corresponding boundary conditions are reduced to a ‘fundamental nucleo’ in terms of the displacement components. The fundamental nucleo does not depend upon the approximation order. It is, therefore, assumed as a free parameter of the formulation. This scheme is named Carrera’s Unified Formulation [22].

Higher-order beam theories can easily be implemented on the basis of the Carrera Unified Formulation, and the accuracy of a large variety of beam theories can be established in a hierarchical and/or axiomatic or asymptotic sense.Amodern form of beam theories can therefore be constructed in a hierarchical manner. The number of unknown variables is a free parameter of the problem. A 3D stress/strain field can be obtained by an appropriate choice of these variables for any type of beam problem: compact sections, thin-walled sections, bending, torsion, shear, localized loadings, static

and dynamic problems [23]. More details and assessments concerning this unified formulation can be found in the works of Carrera and co-workers [24–27].

In this paper, the linear static analysis of a rectangular cantilever beam with a hole of different sizes on its cross-section uses the Carrera Unified Formulation (CUF) and both Taylor and Lagrange expansion modelling approaches. To obtain the governing equations and the Finite Element formulation, the Principle of Virtual Displacements is employed. First, a study of convergence and assessment with available results is done so as to evaluate the stability of the outcomes. Afterwards, consideration is given separately to a cantilevered beam with compact cross-section, and for the presence of a hole with different radius sizes on its cross-section, subjected to vertical concentrated load. The outcomes obtained are introduced by means of figures and tables.

2. The carrera unified formulation (CUF) and finite element formulation

Consider a beam with length L, width b, and thickness h. The rectangular Cartesian coordinate system is presented in Figure 1. Assume that the beam occupies the region:

$$-b/2 \le x \le b/2\,, 0 \le y \le L, -h/2 \le z \le h/2 \tag{1}$$

The general displacement vector is:

$$u(x,y,z) = [u_x \quad u_y \quad u_z]^T \tag{2}$$

The stress, σ_{ij}, and strain, ε_{ij}, components are grouped as follows:

$$\begin{aligned} &\sigma_p = [\sigma_{zz} \quad \sigma_{xx} \quad \sigma_{zx}]^T, \varepsilon_p = [\varepsilon_{zz} \quad \varepsilon_{xx} \quad \varepsilon_{zx}]^T \\ &\sigma_n = [\sigma_{zy} \quad \sigma_{xy} \quad \sigma_{yy}]^T, \varepsilon_n = [\varepsilon_{zy} \quad \varepsilon_{xy} \quad \varepsilon_{yy}]^T \end{aligned} \tag{3}$$

In Eq. (3), the subscript ‘‘p’’ represents the terms lying on planes orthogonal to the cross-section, while ‘‘n″ represents the terms lying on the cross-section. In the case of small displacement, the strain- displacement relations are expressed as

$$\begin{aligned} &\varepsilon_p = D_p u \\ &\varepsilon_n = D_n u = \left(D_{n\Omega} + D_{ny}\right) u \end{aligned} \tag{4}$$

where Ω is the symbol denoting the cross-sectional plane of the beam, and D_p, $D_{n\Omega}$, and D_{ny} are symbols denoting the linear differential operators given as follows:

$$D_p = \begin{bmatrix} 0 & 0 & \frac{\partial}{\partial z} \\ \frac{\partial}{\partial x} & 0 & 0 \\ \frac{\partial}{\partial z} & 0 & \frac{\partial}{\partial x} \end{bmatrix}, D_{n\Omega} = \begin{bmatrix} 0 & \frac{\partial}{\partial z} & 0 \\ 0 & \frac{\partial}{\partial x} & 0 \\ 0 & 0 & 0 \end{bmatrix}, D_{n\Omega} = \begin{bmatrix} 0 & 0 & \frac{\partial}{\partial y} \\ \frac{\partial}{\partial y} & 0 & 0 \\ 0 & \frac{\partial}{\partial y} & 0 \end{bmatrix} \tag{5}$$

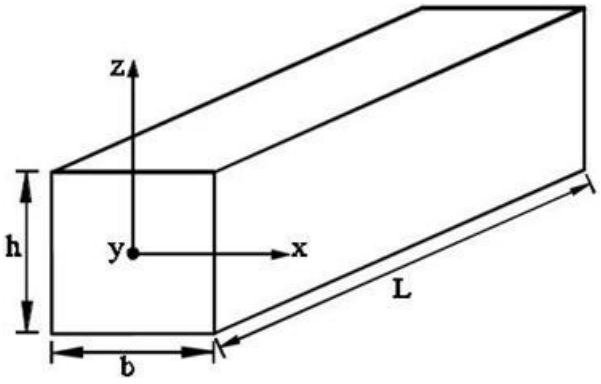

Figure 1. Coordinate system of beam model

The constitutive equations with respect to Hooke's law are given by

$$\sigma = C\varepsilon \tag{6}$$

In Eq. (6), the following notation is used: σ is the stress vector, ε is the strain vector, and C is Hooke's law stiffness matrix. By using Eq. (3), Eq. (6) can be expressed as follows:

$$\sigma_p = \tilde{C}_{pp}\varepsilon_p + \tilde{C}_{pn}\varepsilon_n, \sigma_n = \tilde{C}_{np}\varepsilon_p + \tilde{C}_{nn}\varepsilon_n \tag{7}$$

In the case of an isotropic material, the matrices $\tilde{C}_{pp}$, $\tilde{C}_{pn}$, $\tilde{C}_{np}$, and $\tilde{C}_{nn}$ are expressed as follows:

$$\tilde{C}_{pp} = \begin{bmatrix} \tilde{C}_{11} & \tilde{C}_{12} & 0 \\ \tilde{C}_{12} & \tilde{C}_{22} & 0 \\ 0 & 0 & \tilde{C}_{66} \end{bmatrix}, \ \tilde{C}_{pn} = \tilde{C}_{np}^T = \begin{bmatrix} 0 & 0 & \tilde{C}_{13} \\ 0 & 0 & \tilde{C}_{23} \\ 0 & 0 & 0 \end{bmatrix}, \ \tilde{C}_{nn} = \begin{bmatrix} \tilde{C}_{55} & 0 & 0 \\ 0 & \tilde{C}_{44} & 0 \\ 0 & 0 & \tilde{C}_{33} \end{bmatrix} \tag{8}$$

The coefficients of matrix $\left[\tilde{C}\right]_{ij}$ depend on the material properties and can be obtained as a particular case of orthotropic material [28].

Within the scope of the Carrera Unified Formulation (CUF), the 3D displacement field can be expressed as follows:

$$u = F_\tau(x,z)u_\tau(y), \qquad \tau = 1,2,3,\dots\dots,M = M(N) \tag{9}$$

In Eq. (9), $F_\tau(x,z)$ are the expansion functions with respect to the coordinates x and z on the cross-section, $u_\tau(y)$ is the vector of the generalized displacements depending on the beam axis, M is the number of terms used in the expansion, the repeated indexes τ denote summation according to the Einstein notation, and N is the expansion order and a free parameter of the formulation. The choice of the expansion functions $F_\tau(x,z)$ and the number of terms M is completely arbitrary, in other words, different classes of functions of any order can be taken into account to model the displacement field of a structure above its cross-section. In this paper, both Taylor-like and Lagrange polynomials are used to describe the expansion functions $F_\tau(x,z)$. In the Taylor-like case, as the expansion order N increases, the number of terms M increases as well, and non-classical effects, such as in-and out-of-plane warping of the cross-section, torsion, and transverse shear deformation are accounted for. The expansion functions $F_\tau(x,z)$ are considered to

consist of Mac Laurin's polynomials. The expansion order N defines the polynomial order. However, in the case of Lagrange expansions, the polynominal order is defined by the number of nodes taken on the cross-section.
The vector of generalized displacements $u_\tau(y)$ can be interpolated by means of the shape function $N_i(y)$ as follows:

$$u_\tau(y) = N_i(y) q_{\tau i}, \quad i = 1, 2, \ldots\ldots, N_{NE} \tag{10}$$

where $q_{\tau i}$ is the vector of nodal displacement, and N_{NE} is the number of nodes on the element. The shape functions $N_i(y)$ are not given here, as they are well-known from the literature [29].

In this paper, 1D finite elements with four nodes ($B4$) (that is, a cubic approximation along the beam axis y) and nine-node Lagrange elements are used. It should be noted that the number of nodes per element, N_{NE}, depends on the convergence along the beam axis, y, while the beam model order, N, depends on the expansion on the cross-section. These are not related to each other and are completely independent.

In the static case, the principle of virtual displacements can be written as follows:

$$\delta L_{int} = \int \left(\delta \varepsilon_p^T \sigma_p + \delta \varepsilon_n^T \sigma_n \right) dV = \delta L_{ext} \tag{11}$$

where δ, L_{int}, and L_{ext} are the virtual variation operator, the strain energy, and the external work, respectively. After substituting Eqs. (4), (7), (9), and (10) into Eq. (11) , the following expression is obtained:

$$\delta L_{int} = \delta q_{\tau i}^T K^{ij\tau s} q_{sj} \tag{12}$$

where $K^{ij\tau s}$ is the stiffness matrix and for the sake of completeness, its components can be seen in [30].

3. Numerical results

3.1. Convergence studies

Before analyzing the numerical results, a study of the convergence and assessment with available results is performed. For this purpose, a rectangular cantilever beam subjected to a vertical compressive force at the centroid of the end cross-section is considered.
The study is carried out first for the case of compact cross-section and then for the cases of a hole on its cross-section.

For the convergence study, the maximum vertical displacement, u_z, computed at the centroid of the end cross-section is considered. An exact three-dimensional solution obtained by [31] is given in the following formula:

$$u_z = PL^3 / 3EI_x \tag{13}$$

3.1.1. Case 1: Compact cross-section

The geometry of the considered beam, the magnitude of the load, and the parameters of the material of the beam are chosen as follows. The cross-section edge dimensions, b and h, are equal to 0.04 m and 0.03 m, respectively. The length of the considered beam, L, is equal to 1 m. The magnitude of the load, P, is equal to 100 N. The beam is made of isotropic materials. Young's modulus, E, is considered to be 10 GPa, and Poisson's ratio, ν, is considered to be 0.25.

Compared results are shown in Table 1 which shows both the effect of the number of elements in the axial discretization and the different refined beam models on maximum vertical displacement, u_z, which is at the point [0,L,0] of the beam considered.

As the number of elements in the axial discretization and also the expansion order increase for both Lagrange and Taylor type models, a sufficient alliance is observed between the numerical results and those obtained from the exact solution.
It should be noted that four-node cubical elements (B4) in the axial discretization, and nine-node quadrilateral Lagrange elements (L9) on the cross-section discretization are used.

Table 1. Convergence of maximum vertical displacement, u_z, at the point $[0, L, 0]$ for the compact cross-section case.

Axial discretization (number of elements)	$-\boldsymbol{u_z \times 10^{-1}}$ $(\boldsymbol{m})$								
	Beam Models								**Ref.Sol. Eq. (13)**
	Lagrange Expansion			**Taylor Expansion**					
	$1\ L9$	$2\ L9$	$3\ L9$	$N=1$	$N=2$	$N=3$	$N=4$	$N=5$	
$1\ B4$	0.3580	0.3581	0.3581	0.3705	0.3580	0.3581	0.3581	0.3581	0.3703
$10\ B4$	0.3690	0.3691	0.3691	0.3705	0.3690	0.3691	0.3691	0.3691	
$20\ B4$	0.3695	0.3696	0.3696	0.3705	0.3695	0.3696	0.3696	0.3696	
$30\ B4$	0.3696	0.3697	0.3697	0.3705	0.3696	0.3697	0.3697	0.3697	
$40\ B4$	0.3697	0.3697	0.3697	0.3705	0.3697	0.3697	0.3698	0.3698	
$45\ B4$	0.3697	0.3697	0.3698	0.3705	0.3697	0.3697	0.3698	0.3698	

According to the convergence study for the compact rectangular case, a total of $40\ B4$ mesh elements in the axial discretization and $1\ L9$ Lagrange element on the cross-section is chosen. Figure 2 shows the Taylor and Lagrange Expansion modelling approaches for the 3D beam with compact cross-section. In the Taylor Expansion modelling approach, an axis is defined and used to create the Finite Element discretization. However, in the Lagrange Expansion modelling approach, the cross-section nodes can be directly located along the surface contour of the 3D structure [32].

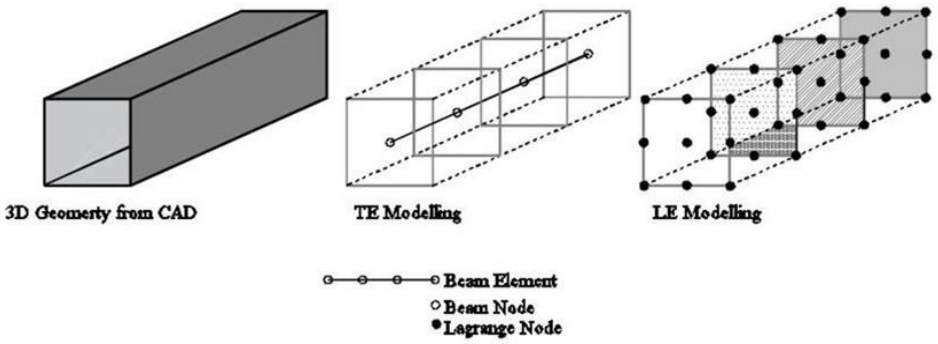

Figure 2. Geometrical considerations of the TE and LE modelling approaches.

3.1.2. Case 2: Cross-section with a hole

A hole with radius r on the cross-section is considered and shown in Figure 3. In the numerical investigations, two cases are considered (where r=0.003 m and r=0.005 m) and a total of 40 B4 mesh elements in the axial discretization and 40 L9 Lagrange elements is used on the cross-section for the best convergence. It should be noted that in order to provide the most appropriate convergence, the discretization procedure on the cross-section is made by the packet program ABAQUS. The numerical results obtained are given as follows. As can be seen from Table 2 and Table 3, a sufficient alliance is observed between the numerical results and those obtained from the exact solution. Figure 4 shows 40 L9 Lagrange elements on a cross-section with a hole.

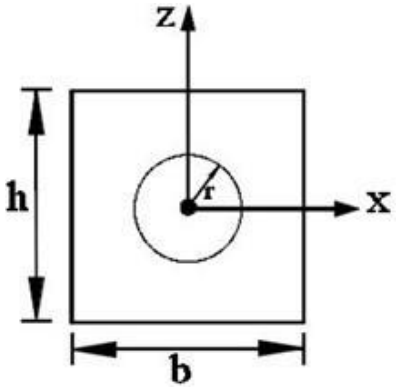

Figure 3. The geometry of cross-section with a hole.

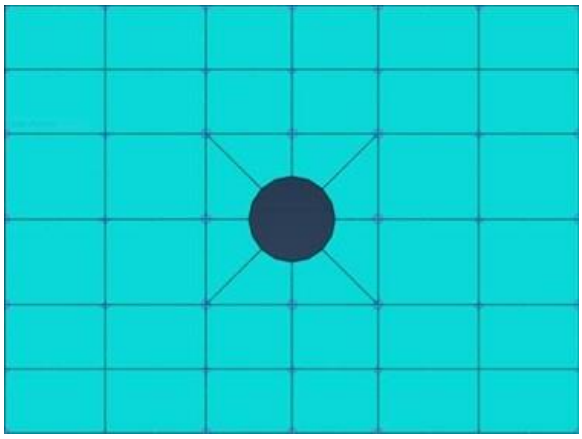

Figure 4. Lagrange Expansion Modelling on the cross-section with a hole.

Table 2. Convergence of maximum vertical displacement,u_z, at the point $[0, L, 0]$ for the case of $r = 0.003\ m$.

Axial discretization (number of elements)	$-\boldsymbol{u_z \times 10^{-1}}$ $(\boldsymbol{m})$						
	Beam Models						**Ref. Sol. Eq. (13)**
	Lagrange Expansion	**Taylor Expansion**					
	40 $L9$	$N = 1$	$N = 2$	$N = 3$	$N = 4$	$N = 5$	
40 $B4$	0.3702	0.3708	0.3699	0.3700	0.3700	0.3701	0.3706

Table 3. Convergence of maximum vertical displacement,u_z, at the point $[0, L, 0]$ for the case of $r = 0.005\ m$.

Axial discretization (number of elements)	$-\boldsymbol{u_z \times 10^{-1}}$ $(\boldsymbol{m})$						
	Beam Models						**Ref. Sol. Eq. (13)**
	Lagrange Expansion	**Taylor Expansion**					
	40 $L9$	$N = 1$	$N = 2$	$N = 3$	$N = 4$	$N = 5$	
40 $B4$	0.3720	0.3725	0.3716	0.3717	0.3718	0.3718	0.3724

3.2. Convergence studies

Thus, after the studies of the convergence and assessment with available results, the problem can now be considered. The following cases are examined.

3.2.1. Case 1: Compact cross-section

The beam is chosen as mentioned before, except for the application point of the load which is at $[0, L, h/2]$. The numerical results obtained are as follows:

Figure 5 shows the maximum values of the axial stress component σ_{yy} at the point of clamped support $(y = 0)$ for a beam subjected to a vertical concentrated load for different refined beam models. As is seen, the role of the higher-order model (Taylor type model) is considerably more obvious than the Lagrange type model especially at $x = \pm b/2, z = \pm h/2$. Figure 6 shows the maximum values of the shear stress component σ_{yz} at the midpoint of the beam $(y = L/2)$ for the same loading case for different refined beam models. As can be seen, the effect of the higher-order model here is also clearly evident.

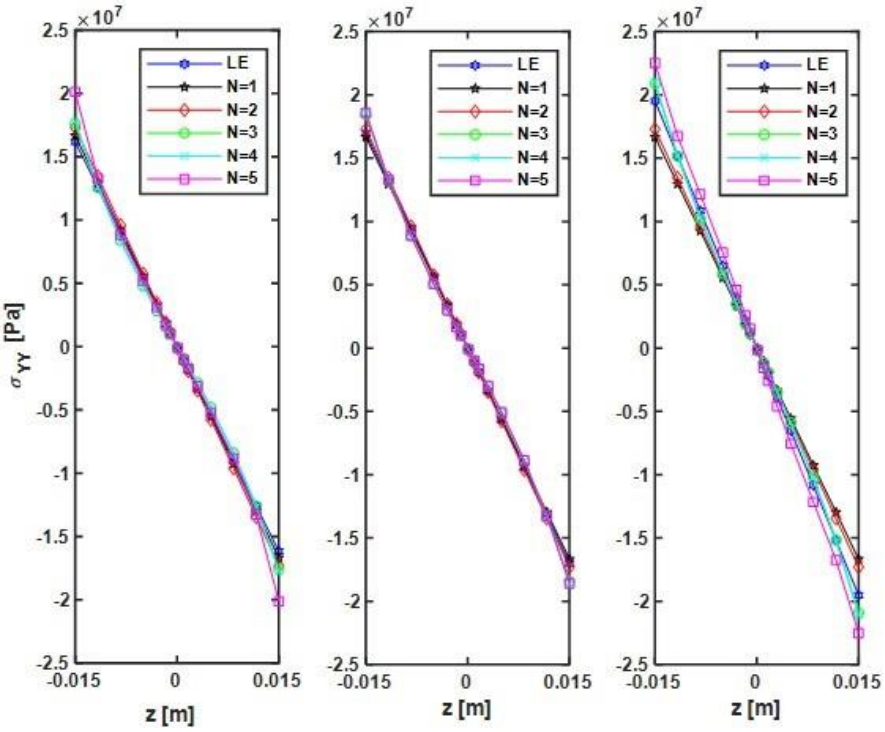

Figure 5. Distribution of maximum axial stress component, σ_{yy}, at $y = 0$ for different refined beam models for (a) at $x = 0$, (b) at $x = \pm b/4$, (c) at $x = \pm b/2$.

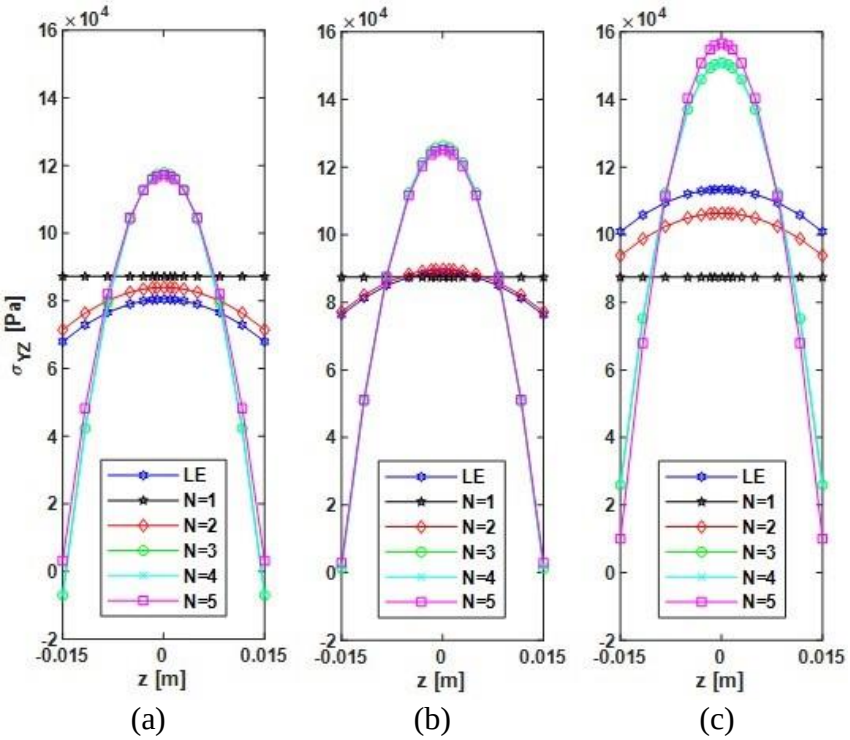

Figure 6. Distribution of maximum shear stress component, σ_{yz}, at $y = L/2$ for different refined beam models for (a) at $x = 0$, (b) at $x = \pm b/4$, (c) at $x = \pm b/2$.

Tables 4 and 5 show the maximum values of axial and shear stress components for different refined beam models.

Table 4. Comparison of maximum axial stress component, σ_{yy}, obtained by using different refined beam models.

Model	$\boldsymbol{y = 0, z = -h/2}$		
	$\boldsymbol{(\sigma_{yy})_{max} \times 10^{7}(Pa)}$		
	$\boldsymbol{x = 0}$	$\boldsymbol{x = \pm b/4}$	$\boldsymbol{x = \pm b/2}$
LE	1.6161	1.7000	1.9519
$\boldsymbol{N = 1}$	1.6666	1.6666	1.6666
$\boldsymbol{N = 2}$	1.7293	1.7293	1.7293
$\boldsymbol{N = 3}$	1.7601	1.8423	2.0893
$\boldsymbol{N = 4}$	1.7759	1.8587	2.1075
$\boldsymbol{N = 5}$	2.0115	1.8523	2.2516

Table 5. Comparison of maximum shear stress component,σ_{yz}, obtained by using different refined beam models.

Model	$\boldsymbol{y = L/2\,, z = 0}$		
	$\boldsymbol{(\sigma_{yz})_{max} \times 10^{4}(Pa)}$		
	$\boldsymbol{x = 0}$	$\boldsymbol{x = \pm b/4}$	$\boldsymbol{x = \pm b/2}$
LE	8.0453	8.8827	11.3400
$\boldsymbol{N = 1}$	8.7209	8.7400	8.8700
$\boldsymbol{N = 2}$	8.3975	8.9712	10.6370
$\boldsymbol{N = 3}$	10.7950	12.6320	15.0900
$\boldsymbol{N = 4}$	11.7950	12.6320	15.0900
$\boldsymbol{N = 5}$	11.7280	12.5190	15.6620

3.2.2.Case 2: Cross-section with a hole
The case of r=0.003 m:

Figure 7 shows the maximum values of the axial stress component σ_{yy} at the point of clamped support $(y = 0)$, and Figure 8 shows the maximum values of the shear stress component σ_{yz} at the midpoint of the beam $(y = L/2)$ for the same loading and for different refined beam models.

As can be seen from both figures, the effect of higher-order beam models on the values of the stress components, σ_yy and σ_yz, is also quite evident in the case of holes. The stress component values obtained in the case of a hole are larger than those obtained for the case where the cross-section is without a hole, most especially for the shear stress component. The stress component values in the hole region on the cross-section must be zero, as expected. However, there must be a sudden jump for the stress components just above the hole. The obtained results are as expected.

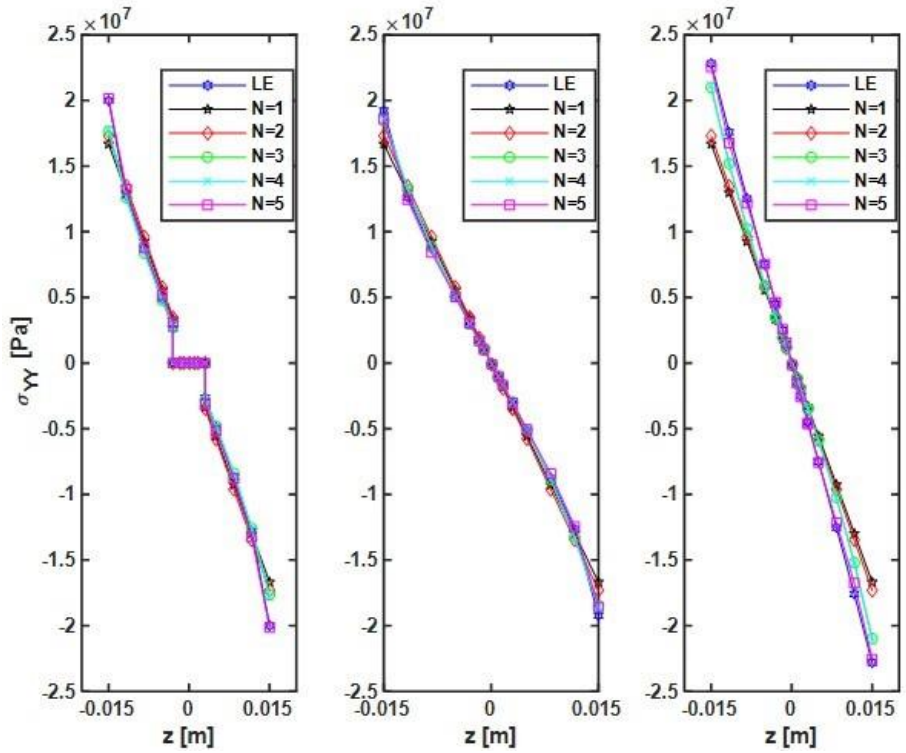

Figure 7. Distribution of maximum axial stress component, σ_{yy}, at $y = 0$ for different refined beam models for **(a)** at $x = 0$, **(b)** at $x = \pm b/4$, **(c)** at $x = \pm b/2$.

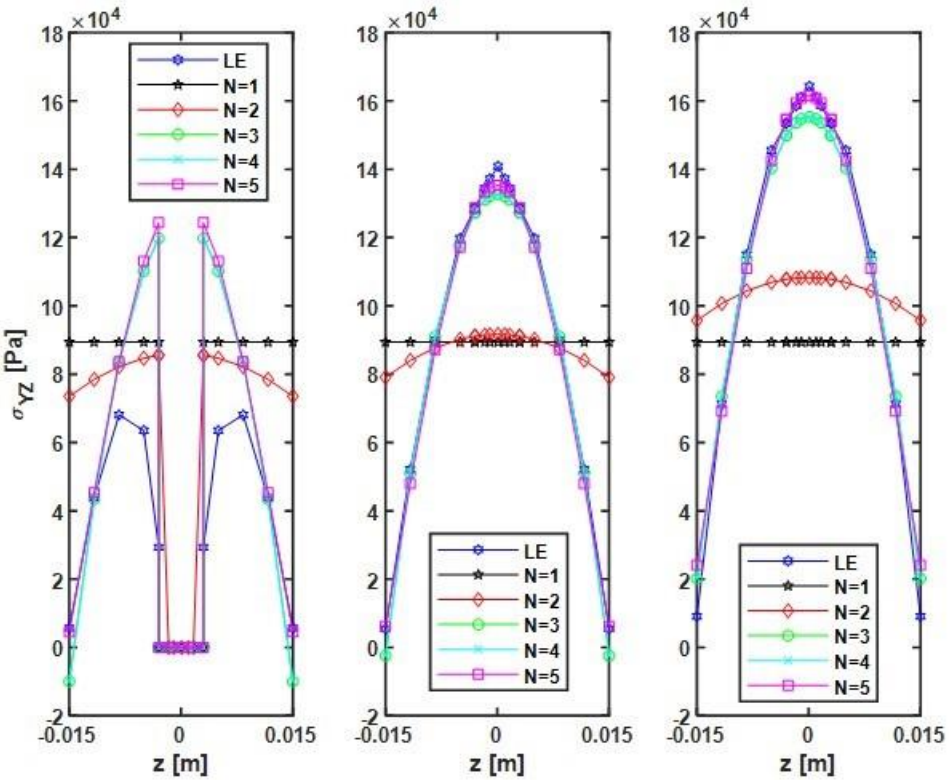

(a) (b) (c)

Figure 8. Distribution of maximum shear stress component, σ_{yz}, at $y = L/2$ for different refined beam models for **(a)** at $x = 0$, **(b)** at $x = \pm b/4$, **(c)** at $x = \pm b/2$.

Tables 6 and 7 show the maximum values of axial and shear stress components for the case of $r = 0.003\ m$ for different refined beam models.

Table 6. Comparison of maximum axial stress component, σ_{yy}, obtained by using different refined beam models.

Model	$\boldsymbol{y = 0, z = -h/2}$		
	$\boldsymbol{(\sigma_{yy})_{max} \times 10^7 (Pa)}$		
	$\boldsymbol{x = 0}$	$\boldsymbol{x = \pm b/4}$	$\boldsymbol{x = \pm b/2}$
LE	1.9987	1.9215	2.2811
$\boldsymbol{N = 1}$	1.6677	1.6677	1.6677
$\boldsymbol{N = 2}$	1.7308	1.7308	1.7308
$\boldsymbol{N = 3}$	1.7634	1.8420	2.0980
$\boldsymbol{N = 4}$	1.7788	1.8627	2.1148
$\boldsymbol{N = 5}$	2.0141	1.8569	2.2542

Table 7. Comparison of maximum shear stress component,σ_{yz}, obtained by using different refined beam models.

Model	$y = L/2, z = 0$		
	$(\sigma_{yz})_{max} \times 10^4 (Pa)$		
	$x = 0$	$x = \pm b/4$	$x = \pm b/2$
LE	0	14.0900	16.4290
$N = 1$	0	8.9395	8.9395
$N = 2$	0	9.1630	10.8300
$N = 3$	0	13.2730	15.5320
$N = 4$	0	13.2730	15.5320
$N = 5$	0	13.5320	16.1619

The case of $r = 0.005\ m$:

Figure 9 shows the maximum values of the axial stress component σ_{yy} at the point of clamped support $(y = 0)$, and Figure 10 shows the maximum values of the shear stress component σ_{yz} at the midpoint of the beam $(y = L/2)$ for the same loading and for different refined beam models. The results obtained are shown below. Concerning the results obtained, similar comments can be made as with the previous case.

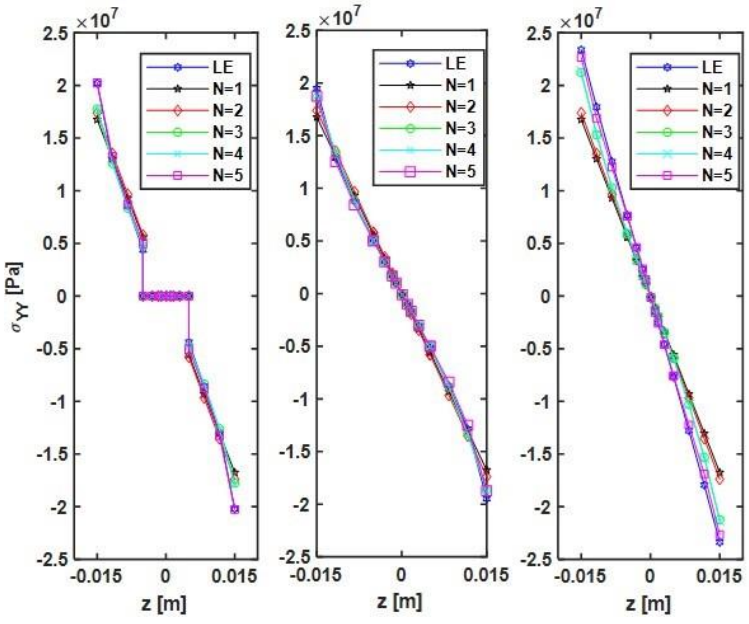

(a) (b) (c)

Figure 9. Distribution of maximum axial stress component, σ_{yy}, at $y = 0$ for different refined beam models for (a) at $x = 0$, (b) at $x = \pm b/4$, (c) at $x = \pm b/2$.

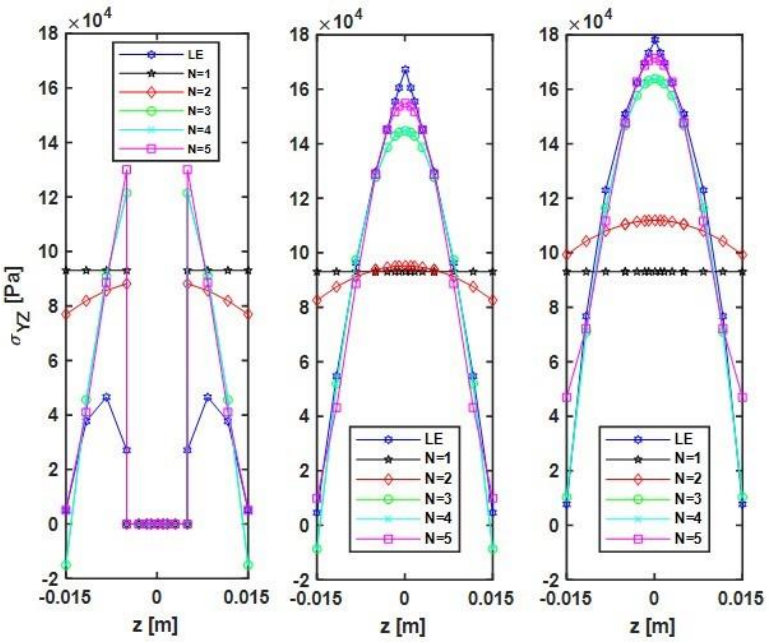

Figure 10. Distribution of maximum shear stress component, σ_{yz}, at $y = L/2$ for different refined beam models for **(a)** at $x = 0$, **(b)** at $x = \pm b/4$, **(c)** at $x = \pm b/2$.

Tables 8 and 9 show the maximum values of axial and shear stress components for the case of $r = 0.005\ m$ for different refined beam models.

Table 8. Comparison of maximum axial stress component, σ_{yy}, obtained by using different refined beam models.

Model	$\boldsymbol{y = 0, z = -h/2}$		
	$\boldsymbol{(\sigma_{yy})_{max} \times 10^7 (Pa)}$		
	$\boldsymbol{x = 0}$	$\boldsymbol{x = \pm b/4}$	$\boldsymbol{x = \pm b/2}$
LE	2.0213	1.9469	2.3387
$\boldsymbol{N = 1}$	1.6757	1.6757	1.6757
$\boldsymbol{N = 2}$	1.7395	1.7395	1.7395
$\boldsymbol{N = 3}$	1.7753	1.8625	2.1243
$\boldsymbol{N = 4}$	1.7903	1.8773	2.1385
$\boldsymbol{N = 5}$	2.0258	1.8722	2.2666

Table 9. Comparison of maximum shear stress component,σ_{yz}, obtained by using different refined beam models.

Model	$y = L/2\,, z = 0$		
	$(\sigma_{yz})_{max} \times 10^4 (Pa)$		
	$x = 0$	$x = \pm b/4$	$x = \pm b/2$
LE	0	16.7260	17.8143
$N = 1$	0	9.3060	9.3060
$N = 2$	0	9.5157	11.1906
$N = 3$	0	14.4833	16.3866
$N = 4$	0	14.4833	16.3865
$N = 5$	0	15.4835	17.1510

In this paper, the effect of both the use of different order beam models and the presence of a hole on the cross-section on the stress distribution were investigated. For the Lagrange expansion model, according to the results obtained, the most significant difference for both the maximum axial stress component, σ_{yy}, and maximum shear stress component, σ_{yz}, is seen on the cross-section at the point $x = \pm b/2$. This is illustrated by the following Figure 11 and Figure 12.

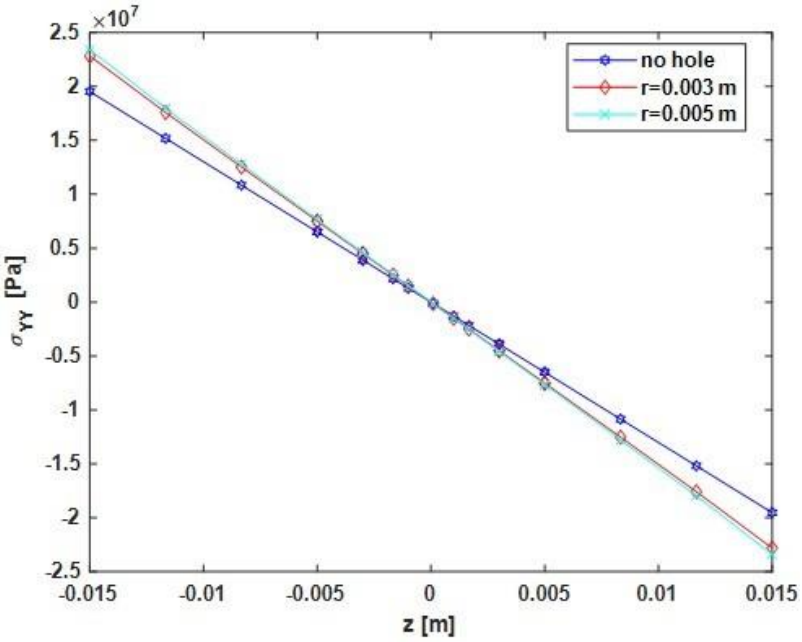

Figure 11. Distribution of maximum axial stress component, σ_{yy}, at $x = \pm b/2$, $y = 0$ for Lagrange Expansion model (LE).

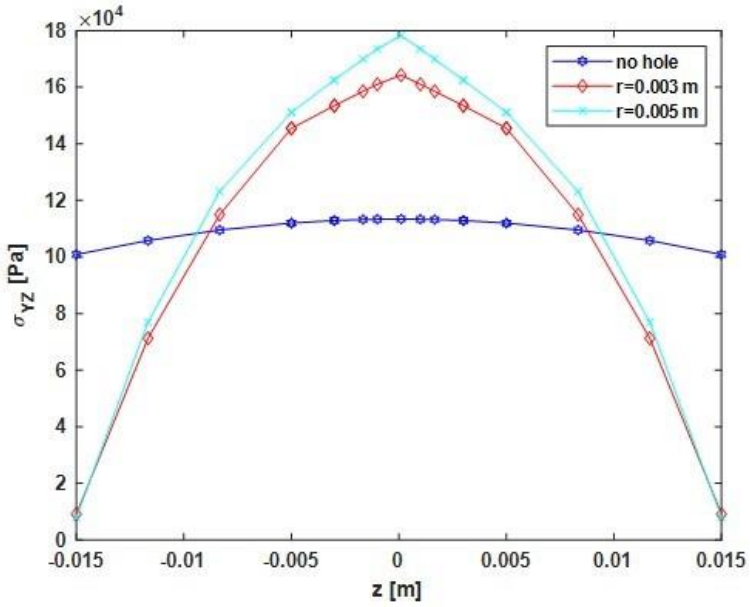

Figure 12. Distribution of maximum shear stress component, σ_{yz}, at $x = \pm b/2, y = L/2$ for Lagrange Expansion model (LE).

4. Conclusions

According to the foregoing analyses, the following main conclusions can be drawn:

- In the case of compact cross-section, for the maximum axial stress component ,σ_{yy}, at the point of clamped support $(y = 0)$, the role of the higher-order model (Taylor type model) is considerably more obvious than the Lagrange type model (LE) (Fig. 5).

- In the case of compact rectangular cross-section, for the maximum shear stress component, σ_{yz}, at the midpoint of the beam $(y = L/2)$, the role of the higher-order model (Taylor type model) is considerably more obvious than the Lagrange type model (LE) (Fig. 6).

- In the case of a small hole, as expected, the stress component values (σ_{yy} and σ_{yz}) obtained are larger than those obtained in the case where the cross-section is without a hole, most especially for the shear stress component (σ_{yz}).

- In the case of a small hole, for the maximum axial stress component ,σ_{yy}, at the point of clamped support $(y = 0)$, the role of the Lagrange type model is considerably more obvious than the higher-order model (Taylor type model) (Fig. 7 and Fig. 9).

- In the case of a small hole, for the maximum shear stress component ,σ_{yz}, at the midpoint of the beam $(y = L/2)$, the role of the Lagrange type model is considerably more obvious than the higher-order model (Taylor type model) (Fig. 8 and Fig. 10).

- It can be said that the use of Lagrange type expansions above the cross-section represents an attractive solution to capture non-classical, local phenomena on the cross-section.

References

[1] Timoshenko, S.P., On the corrections for shear of the differential equation for transverse vibrations of prismatic bars, **Philosophical Magazine**, 41, 744-746, (1921).

[2] Cowper, G.R., The shear coefficient in Timoshenko's beam theory, **Journal of Applied Mechanics**, 33,2, 335-340, (1966).

[3] Pai, P.F. and Schulz, M.J., Shear correction factors and an energy consistent beam theory, **International Journal of Solids and Structures**, 36, 1523-1540, (1999).

[4] Gruttmann, F., et al., Shear stresses in prismatic beams with arbitrary cross-sections, **International Journal for Numerical Methods in Engineering**, 45, 865-889, (1999).

[5] Gruttmann, F., and Wagner, W., Shear correction factors in Tmoshenko's beam theory for arbitrary shaped cross-section, **Computational Mechanics**, 27, 199-207, (2001).

[6] Hutchinson, J.R., Transverse vibrations of beams, exact versus approximate solutions, **Journal of Applied Mechanics-Transactions of the Asme**, 48,4, 923-928, (1981).

[7] Rychter, Z., On the shear coefficient in beam bending, **Mechanics Research Communications**, 14,5–6, 379–385, (1987).

[8] Mechab, I., et al., Deformation of short composite beam using refined theories, **Journal of Mathematical Analysis and Applications**, 346, 468-479, (2008).

[9] Dong, S.B., et al., Much ado about shear correction factors in Timoshenko beam theory, **International Journal Of Solids And Structures**, 47,13,, 1651-1665, (2010).

[10] Mucichescu, D.T., Bounds for stiffness of prismatic beams, **Journal of Structural Engineering**, 110, 1410-1414, (1984).

[11] Bekhadda, A., et al., Static buckling and vibration analysis of continuously graded ceramic-metal beams using a refined higher order shear deformation theory, **Multidiscipline Modeling In Materials And Structures**, 15,6, 1152-1169, (2019).

[12] Rajagopal, A., Variational Asymptotic Based Shear Correction Factor for Isotropic Circular Tubes, **AIAA Journal**, 57,10, 4125-4131, (2019).

[13] Wagner, W., and Gruttmann, F., A displacement method for the analysis of flexural shear stresses in thin-walled isotropic composite beams, **Computers & Structures**, 80,24, 1843-1851, (2002).

[14] Cai, J., and Moen, C.D., Elastic buckling analysis of thin-walled structural members with rectangular holes using generalized beam theory, **Thin-Walled Structures**, 107, 274-286, (2016).

[15] Taig, G., and Ranzi, G., Generalised Beam Theory (GBT) for composite beams with partial shear interaction, **Engineering Structures**, 99, 582-602, (2015).

[16] Carrera, E., Pagani, A., Petrolo, M., et al., Recent developments on refined theories for beams with applications, **Mechanical Engineering Reviews**, 2,2, (2015).

[17] Liu, L., and Lu, N., Variational formulations, instabilities and critical loadings of space curved beams, **International Journal Of Solids And Structures**, 87, 48-60, (2016).

[18] Pagani, A., and Carrera, E., Unified formulation of geometrically nonlinear refined beam theories, **Mechanics Of Advanced Materials And Structures**, 25,1, 15-31, (2018).

[19] Carrera, E., de Miguel, A. G., and Pagani, A., Extension of MITC to higher-order beam models and shear locking analysis for compact, thin-walled, and composite structures, **International Journal For Numerical Methods In Engineering**, 112,13, 1889-1908, (2017).

[20] Carrera, E., and Zappino, E., One-dimensional finite element formulation with node-dependent kinematics, **Computers & Structures**, 192, 114-125, (2017).

[21] Richard, S., Generalized Beam Theory-an adequate method for coupled stability problems, **Thin-Walled Strcut**, 19,2-4, 161-80, (1994).

[22] Carrera, E., and Giunta, G., Refined beam theories based on a unified formulation, **International Journal of Applied Mechanics**, 2,1, 117-143, (2010).

[23] Carrera, E., Giunta, G., and Petrolo, M., **Beam Structures Classical and Advanced Theories**, A John Wiley & Sons, Ltd., Publication, (2011).

[24] Karataş, E.E., Filippi, M., and Carrera, E., Dynamic analyses of viscoelastic three-dimensional structures with advanced one-dimensional finite elements, **European Journal of Mechanics/A Solids**, 88, (2021).

[25] Carrera, E., and Demirbas, D.M.,Evaluation of bending and post-buckling behavior of thin-walled FG beams in geometrical nonlinear regimewith CUF, **Composite Structures**, 275,(2021).

[26] Carrera, E., Demirbaş, M.D., and Augello, R., Evaluation of Stress Distribution of Isotropic, Composite, and FG Beams with Different Geometries in Nonlinear Regime via Carrera-Unified Formulation and Lagrange Polynomial Expansions, **Applied Scıences-Basel**, 11(22), (2021).

[27] Demirbaş, M.D., Çalışkan, U., Xu, X., and Filippi, M., Evaluation of the bending response of compact and thin-walled FG beams with CUF, MECHANICS OF **Advanced Materials And Structures,** 28(17), (2021).

[28] Reddy, J.N., **Mechanics of laminated composite plates and shells: theory and analysis**, Boca Raton, FL: CRC Press, (2004).

[29] Bathe, K., **Finite element procedure**, Prentice Hall, Englewood Cliffs, NJ, (1996).

[30] Carrera, E., Petrolo, M., and Zappino, E., Performance of CUF Approach to Analyze the Structural Behavior of Slender Bodies, **Journal of Structural Engineering**, 138,2, 284-296, (2012).

[31] Timoshenko, S.P., and Goodier, J.N., **Theory of elasticity**, McGraw-Hill; (1970).

[32] Carrera, E., et al., **Finite Element Analysis of Structures through Unified Formulation**, John Wiley & Sons Ltd, (2014).